Biomedical Optics EXPRESS

Correction of depth-induced spherical aberration for deep observation using two-photon excitation fluorescence microscopy with spatial light modulator

Naoya Matsumoto,[1,*] Takashi Inoue,[1] Akiyuki Matsumoto,[2] and Shigetoshi Okazaki[3]

[1] *Central Research Laboratory, Hamamatsu Photonics K.K., 5000 Hirakuchi, Hamakita-ku, Hamamatsu-City, Shizuoka-Pref., 434-8601, Japan*
[2] *Department of Biochemistry, Nagoya University Graduate School of Medicine, 65 Tsurumai-cho, Showa-ku, Nagoya-City, Aichi-Pref., 466-8550, Japan*
[3] *Department of Medical Spectroscopy, Applied Medical Photonics Laboratory, Medical Photonics Research Center, Hamamatsu University School of Medicine, 1-20-1 Handayama, Higashi-ku, Hamamatsu-City, Shizuoka-Pref., 431-3192, Japan*

[*] *nm@crl.hpk.co.jp*

Abstract: We demonstrate fluorescence imaging with high fluorescence intensity and depth resolution in which depth-induced spherical aberration (SA) caused by refractive-index mismatch between the medium and biological sample is corrected. To reduce the impact of SA, we incorporate a spatial light modulator into a two-photon excitation fluorescence microscope. Consequently, when fluorescent beads in epoxy resin were observed with this method of SA correction, the fluorescence signal of the observed images was ∼27 times higher and extension in the direction of the optical axes was ∼6.5 times shorter at a depth of ∼890 μm. Thus, the proposed method increases the depth observable at high resolution. Further, our results show that the method improved the fluorescence intensity of images of the fluorescent beads and the structure of a biological sample.

OCIS codes: (170.3880) Medical and biological imaging; (170.2520) Fluorescence microscopy; (220.1000) Aberration compensation; (230.6120) Spatial light modulators.

References and links

1. W. Denk, J. H. Strickler, and W. W. Webb, "Two-photon laser scanning fluorescence microscopy," Science **248**, 73–76 (1990).
2. D. Kobat, M. E. Durst, N. Nishimura, A. W. Wong, C. B. Schaffer, and C. Xu, "Deep tissue multiphoton microscopy using longer wavelength excitation," Opt. Express **17**(16) 13354–13364 (2009).
3. P. Theer, M. T. Hasan, and W. Denk, "Two-photon imaging to a depth of 1000 μm in living brains by use of a Ti:Al2O3 regenerative amplifier," Opt. Lett. **28**(12), 1022–1024 (2003).
4. E. J. Botcherby, C. W. Smith, M. M. Kohl, D. Débarre, M. J. Booth, R. Juškaitis, O. Paulsen, and T. Wilson, "Aberration-free three-dimensional multiphoton imaging of neuronal activity at kHz rates," Proc. Natl. Acad. Sci. USA **109**(8), 2919–2924 (2012).
5. X. Tao, B. Fernandez, O. Azucena, M. Fu, D. Garcia, Y. Zuo, D. C. Chen, and J. Kubby, "Adaptive optics confocal microscopy using direct wavefront sensing," Opt. Lett. **36**(7), 1062–1064 (2011).
6. O. Azucena, J. Crest, J. Cao, W. Sullivan, P. Kner, D. Gavel, D. Dillon, S. Olivier, and J. Kubby, "Wavefront aberration measurements and corrections through thick tissue using fluorescentmicrosphere reference beacons," Opt. Express, **18**(16), 17521–17532 (2010).

#237841 Received 9 Apr 2015; revised 11 Jun 2015; accepted 12 Jun 2015; published 17 Jun 2015

7. D. E. Milkie, E. Betzig, and N. Ji, "Pupil-segmentation-based adaptive optical microscopy with full-pupil illumination," Opt. Lett. **36**(21), 4206–4208 (2011).
8. C. Wang, R. Liu, D. E. Milkie, W. Sun, Z. Tan, A. Kerlin, T. W. Chen, D. S. Kim, and N. Ji, "Multiplexed aberration measurement for deep tissue imaging in vivo," Nat. Meth. **11**, 1037–1040 (2014).
9. J. Zeng, P. Mahou, M. C. Schanne-Klein, E. Beaurepaire, and D. Debarre, "3D resolved mapping of optical aberrations in thick tissues," Bio. Opt. Express **3**(8), 1898–1913 (2012).
10. R. Kawakami, K. Sawada, A. Sato, T. Hibi, Y. Kozawa, S. Sato, H. Yokoyama, and T. Nemoto, "Visualizing hippocampal neurons with in vivo two-photon microscopy using a 1030 nm picosecond pulse laser," Sci. Rep. **3**, 1014 (2013)
11. H. Hama, H. Kurokawa, H. Kawano, R. Ando, T. Shimogori, H. Noda, K. Fukami, A. Sakaue-Sawano, and A. Miyawaki, "Scale: A chemical approach for fluorescence imaging and reconstruction of transparent mouse brain," Nat. Neurosci. **14**, 1481–1488 (2011).
12. R. Dickie, R. M. Bachoo, M. A. Rupnick, S. M. Dallabrida, G. M. DeLoid, J. Lai, R. A. DePinho, and R. A. Rogers, "Three-dimensional visualization of microvessel architecture of whole-mount tissue by confocal microscopy," Microvasc. Res. **72**, (1-2), 20–26 (2006).
13. E. A. Susaki, K. Tainaka, D. Perrin, F. Kishino, T. Tawara, T. M. Watanabe, C. Yokoyama, H. Onoe, M. Eguchi, S. Yamaguchi, T. Abe, H. Kiyonari, Y. Shimizu, A. Miyawaki, H. Yokota, and H. R. Ueda, "Whole-brain imaging with single-cell resolution using chemical cocktails and computational analysis," Cell **157**(3), 726–739 (2014).
14. M. T. Ke, S. Fujimoto, and T. Imai, "SeeDB: A simple and morphology-preserving optical clearing agent for neuronal circuit reconstruction," Nat. Neurosci. **16**, 1154–1161 (2013).
15. T. Kuwajima, A. A. Sitko, P. Bhansali, C. Jurgens, W. Guido, and C. Mason, "ClearT: A detergent- and solvent-free clearing method for neuronal and non-neuronal tissue," Development **140**, 1364–1368 (2013).
16. A. Erturk, K. Becker, N. Jahrling, C. P. Mauch, C. D. Hojer, J. G. Egen, F. Hellal, F. Bradke, M. Sheng, and H. U. Dodt, "Three-dimensional imaging of solvent-cleared organs using 3DISCO," Nat. Proto. **7**, 1983–1995 (2012).
17. T. Inoue, H. Tanaka, N. Fukuchi, M. Takumi, N. Matsumoto, T. Hara, N. Yoshida, Y. Igasaki, and Y. Kobayashi, "LCOS spatial light modulator controlled by 12-bit signals for optical phase-only modulation," Proc. SPIE **6487**, 64870Y (2007).
18. N. Matsumoto, T. Ando, T. Inoue, Y. Ohtake, N. Fukuchi, and T. Hara, "Generation of high-quality higher-order Laguerre-Gaussian beams using liquid-crystal-on-silicon spatial light modulators," J. Opt. Soc. Am. A **25**(7), 1642–1651 (2008).
19. P. Török, P. Varga, and G. R. Booker, "Electromagnetic diffraction of light focused through a planar interface between materials of mismatched refractive indices: Structure of the electromagnetic field. I," J. Opt. Soc. Am. A **12**(10), 2136–2144 (1995).
20. P. S. Salter, M. Baum, I. Alexeev, M. Schmidt, and M. J. Booth, "Exploring the depth range for three-dimensional laser machining with aberration correction," Opt. Express **22**(15), 17644–17656 (2014).
21. H. Itoh, N. Matsumoto, and T. Inoue, "Spherical aberration correction suitable for a wavefront controller," Opt. Express **17**(16), 14367–14373 (2009).
22. N. Matsumoto, H. Itoh, T. Inoue, T. Otsu, and H. Toyoda, "Stable and flexible multiple spot pattern generation using LCOS spatial light modulator," Opt. Express **22**(20), 24722–24733 (2014).
23. T. J. Gould, D. Burke, J. Bewersdorf, and M. J. Booth, "Adaptive optics enables 3D STED microscopy in aberating specimens," Opt. Express **20**(19), 20998–21009 (2012).

1. Introduction

Deep-tissue imaging using two-photon excitation fluorescence microscopy (TPM) has attracted considerable attention for the study of the structure and vital functions of the brain owing to its high fluorescence intensity and depth resolution [1,2]. For example, three-dimensional imaging of vessels and neurons has been carried out via observations from the surface of a thick biological sample into deep regions [3, 4]. However, when the deeper regions of a biological sample are observed, the fluorescence intensity and depth resolution are degraded owing to increased aberration, scattering, and absorption [2,3]. Spherical aberration (SA) is caused by the structure of the biological sample and refractive-index (RI) mismatch between the air (or the immersion fluid) and the sample being observed. To reduce SA, water and silicone-oil immersion objective lenses are commonly used to reduce the RI mismatch between the immersion fluid and the sample. Adaptive optics using a spatial light modulator (SLM) and a wavefront sensor has also been studied as an active correction method to reduce the impact of various aberrations [5, 6]. This method iteratively measures the wavefront of a well-known fluorescent object called a

#237841 Received 9 Apr 2015; revised 11 Jun 2015; accepted 12 Jun 2015; published 17 Jun 2015

guide star and modulates the wavefront of the excitation light so that the fluorescence intensity of the guide star is at its maximum. The pupil segmentation method has also been proposed as a method of providing adaptive optics without a wavefront sensor [7–9]. In this method, the pupil is segmented and the wavefront of the excitation light on each segment is modulated in order to maximize the intensity of the guide star. Using this method, in vivo imaging of dendritic spines has been achieved with high resolution [8].

Scattering and absorption are caused by the structure of biological samples. To reduce scattering and absorption, TPM using longer wavelengths [2, 3, 10] and an optical clearing agent [11–16] has been developed. Hama et al. [11] observed neurons in the brain up to a depth of 4 mm by reducing the effects of scattering and absorption. Recently, Scale A2 [11], BABB [12], CUBIC [13], SeeDB [13, 14], ClearT [15], and 3DISCO [16] have been reported as high-quality optical clearing agents, the RI of which depends on the agent and tends to be higher (n = 1.38 – 1.55) than that of water (n = 1.33) and silicone oil (n = 1.408). In general, it is necessary to adopt an objective lens suitable for the agent to carry out observation without aberration caused by RI mismatch. However, it is difficult to adopt an objective lens suitable for every observation condition because other specifications of the objective lens such as numerical aperture (NA), magnitude, and working distance also have to be considered.

In the present study, to observe deep regions while reducing SA caused by RI mismatch, we incorporated an SLM [17, 18] into the TPM system. The SLM modulates the wavefront of the excitation light to a numerically calculated wavefront for correcting SA using certain specifications. Because of the direct calculation involved, the proposed method does not use a guide star. To verify the efficacy of the proposed SA correction method, we demonstrate the observation of fluorescent beads in epoxy resin from the surface to deep regions using a dry objective lens. Further, using the proposed method we observe fluorescent beads in a biological sample and the structure of the biological sample with high fluorescence intensity and depth resolution, even in deep regions.

2. Observation method with SA correction

Figure 1 shows the convergence of a laser beam when the beam is focused inside a medium m_2 such as a biological sample through another medium m_1 such as air and an immersion fluid. In the figure, the geometry of excitation light focused with an objective lens of focal length f and numerical aperture NA is shown. While the RI of the immersion medium n_1 has uniform distribution, the RI of the biomedical sample has the variant distribution. The higher-order aberrations are caused by RI distribution in the biomedical sample, and the lower-order aberrations includingc depth-induced SA are caused by mismatch between n_1 and average RI of the biological sample n_2. Generally, the effect of the lower-order aberrations on the fluorescence intensity is larger than that of higher-order aberrations because the amount of RI change in the biological samples is smaller than the difference of average RI of biological samples from RI of immersion media. Arch AB denotes the reference spherical wavefront when a collimated laser beam is incident on the objective lens. If $n_1 = n_2$ and the wavefront of the collimated laser beam incident on the lens is planar, the beam is converged at point O_0 at a distance d from the interface between m_1 and m_2 (Fig. 1(a)). Under such a condition, the optical depth coincides with the movement of an objective lens from the interface. In the case of $n_1 < n_2$ (Fig. 1(b)), the depth-induced SA originates from RI mismatch between the media. Paraxial rays are focused at shallower points O_1 at a distance $n_2 d/n_1$ (we define O_1 as the optical depth), and peripheral rays are focused at deeper points because the rays are refracted depending on incident angle θ_1 of the ray at the interface (Snell's law). The deeper the focal point is, the larger the SA is. Consequently, the focal spot of the excitation light is elongated in the optical-axis direction, and its power density decreases; the excited fluorescence spot is also extended and its fluorescence

#237841 Received 9 Apr 2015; revised 11 Jun 2015; accepted 12 Jun 2015; published 17 Jun 2015

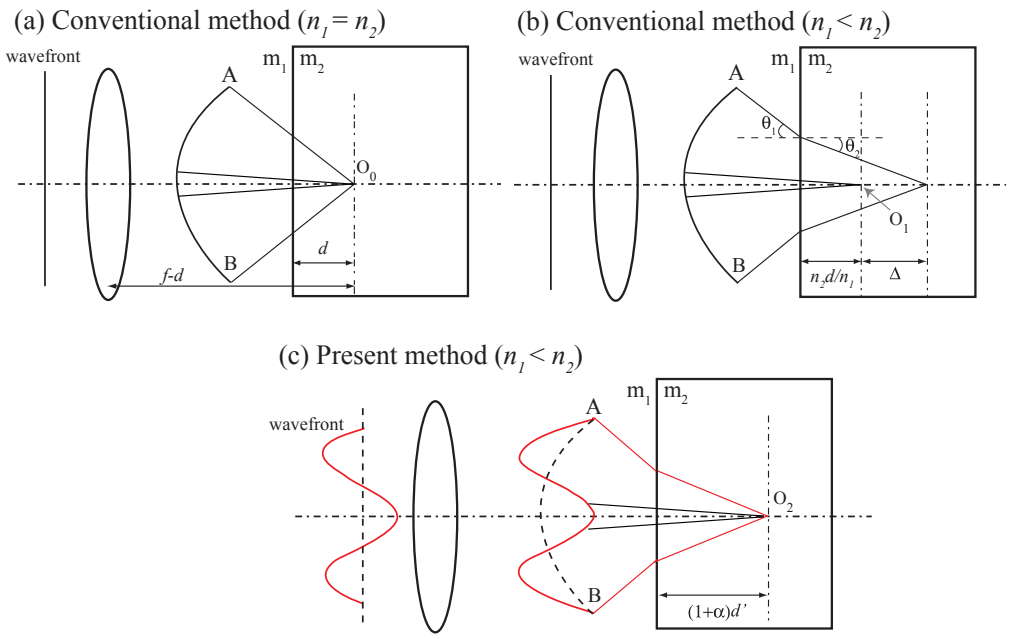

Fig. 1. Focusing geometry showing the refraction of rays at the interface between two media: (a) Rays from a plane wavefront are concentrated at O_0 in the case of $n_1 = n_2$. (b) Rays from a plane wavefront are focused with depth range Δ in the case of $n_1 < n_2$ because the rays are refracted depending on incident angle θ_1 of the ray at the interface (Snell's law). (c) Rays from a modulated wavefront are concentrated at O_2 in the case of $n_1 < n_2$.

intensity becomes weak in deeper regions. The focal spot yields a blurred fluorescence image with low fluorescence intensity and depth resolution.

The SA caused by RI mismatch is expressed as follows [19, 20]:

$$\phi(\rho) = -\frac{2\pi d}{\lambda}\left((1+\alpha)\sqrt{n_2^2-(NA\rho)^2} - \sqrt{n_1^2-(NA\rho)^2}\right), \tag{1}$$

where λ is the wavelength of the excitation light, ρ is the normalized pupil radius, and d is the movement of an objective lens from the interface, and α is the factor for changing the depth of focal spot. This SA can be corrected by modulating the wavefront of excitation light to be the inverse form of Eq. (1). We call this inverse form of Eq. (1) pre-distortion pattern. After applying the pre-distortion pattern to an SLM, the rays inside the sample are concentrated at O_2, at a distance $(1+\alpha)d$ from the interface (Fig. 1(c)). When the wavefront of the excitation light is modulated as shown in Fig. 1(c), paraxial and peripheral rays can be concentrated at the same spot. Consequently, the focal spot of the excitation light is localized, its power density is improved, and fluorescence is excited only at positions near the focal point. As shown in Eq. (1), the pre-distortion pattern is simply calculated using the specifications of the objective lens, movement of the objective lens from the interface between the immersion medium and the sample, the RI of the immersion medium, and the average RI of the sample. Electronic control of the SLM without any mechanical movements enables the numerically calculated wavefront to be applied within a short time period when the movement is changed. Although the excited fluorescence is also affected by SA and its focal spot near the detector plane is widened, we adopt a large light-receiving surface detector such as a photo-multiplier tube (PMT) to reduce the impact of SA. That is, we attempt to correct the SA of excitation light using the

#237841 Received 9 Apr 2015; revised 11 Jun 2015; accepted 12 Jun 2015; published 17 Jun 2015

SLM and minimize the impact of the SA of the fluorescence by using the PMT because a optical sectioning effect is determined by the spot size of the excitation light in TPM. Thus, the fluorescence intensity and the depth resolution of the fluorescence image are improved.

Adaptive optics using an SLM and a wavefront sensor can correct various aberrations including SA. However, with adaptive optics, a well-known fluorescent object called a guide star and a wavefront sensor must be used to measure the wavefront aberrations. If there is no appropriate fluorescent object in the observation area, surgical treatment must be performed to implant a guide star like fluorescent beads. In addition, the adaptive optics requires a short time for observation at each depth because it iteratively performs a feedback process so that the fluorescence intensity of the object becomes highest. In contrast, our proposed method does not use a guide star and wavefront sensor, and we can previously calculate the suitable pre-distortion pattern for each observation depth.

While an objective lens with correction collar can correct both excitation light and fluorescence with high light-utilization efficiency, the controllability of SA correction is low due to mechanical movement. Furthermore, rotation of the correction collar causes unexpected change of the observation depth. In contrast, our proposed method can perform SA correction suitable for each sample and objective lens, as well as adjust the observation depth by adding a defocus wavefront with electrical control [20, 21].

3. Experimental setup

Figure 2 is a simplified schematic showing the setup of our experimental TPM system with an SLM. As shown in the figure, a Ti:sapphire laser (Chameleon Vision II, Coherent Inc.) is used to deliver a horizontally polarized beam of light beam to a beam expander. A femtosecond train of optical pulses (wavelength = 880 nm) is projected onto a small-pixel-pitch LCOS-SLM (1280 $\times$ 1024 pixels, 12.5 μm pixel pitch, Hamamatsu Photonics K.K.) with a Peltier system [22]. The SLM modulates the wavefront of the excitation light to the pre-distortion pattern calculated from Eq. (1). An example of the pre-distortion pattern profile before wrapping has been added to Fig. 2. In fact, a wavefront that superimposes the pre-distortion pattern and correction pattern for the distortion of the SLM is applied to the SLM. The light is reflected and directed through a telecentric lens system to an *x*-*y* galvo scanner. The light with its incident angle varied using the scanner is then directed to an objective lens by the other telecentric lens system. These telecentric lens systems are used to ensure that the wavefront of the light is transmitted from the plane of the SLM to the pupil plane of the objective lens in an inverted microscope system. The light is focused onto a sample by using an objective lens to excite fluorescence, which is gathered by the objective lens. The gathered fluorescence is directed through two telecentric lens systems and the *x*-*y* galvo system to the PMT (Hamamatsu Photonics K. K.). The fluorescence is detected using the PMT. To get the three-dimensional image, scanning is performed at each depth with changing d. At each depth, the pre-distortion pattern is calculated and applied to the SLM. By applying the pre-distortion pattern, the wavefront of excitation light is distorted before incidence on the interface between the immersion medium and the sample. The SA due to RI mismatch is canceled inside the sample by this pre-distortion. Following modulation of the incident light, scanning with SA correction is performed and the fluorescence detected. Conversely, if the pre-distortion pattern is not applied, the functionality of the experimental TPM system becomes equivalent to that of the conventional TPM system.

#237841 Received 9 Apr 2015; revised 11 Jun 2015; accepted 12 Jun 2015; published 17 Jun 2015

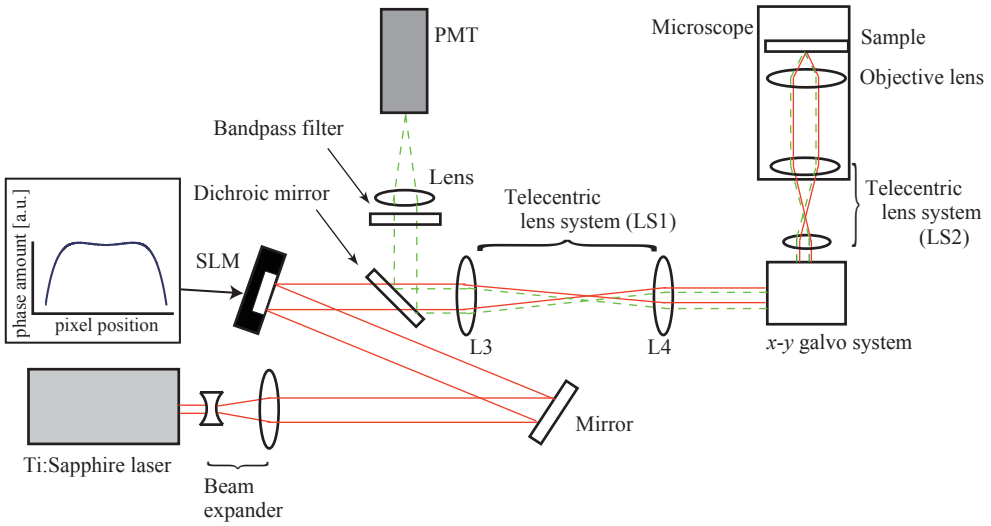

Fig. 2. Schematic of the experimental TPM system with ab SLM. The solid lines (red) and dashed lines (green) represent the excitation beam and fluorescence light, respectively.

4. Experimental results

4.1. Fluorescent polystyrene beads of 3 μm diameter in epoxy resin

We observed 3 μm-diameter fluorescent polystyrene beads in epoxy resin using the experimental system outlined above. The RI of the epoxy resin was approximately 1.55, which is close to that of optical clearing agents (n=1.38 – 1.55). The interface between medium 1 (air, n_1 = 1) and medium2 (epoxy resin, n_2 = 1.55) was flat because there was a cover glass between the air and the epoxy resin. Further, the aberration caused by the cover glass was minimized by using an objective lens with cover glass correction. As a result, the effect of SA caused by RI mismatch between the air and the epoxy resin was dominant. We carried out scanning from the surface of the epoxy resin to the limit of the working distance of the objective lens using a dry objective lens (20$\times$ magnification, NA 0.75, 600 μm working distance, Olympus) with optical-depth increments of 621 nm. The intensity of the excitation light was fixed at 11 mW at the sample position during scanning. At each depth, scanning with SA correction was performed after scanning without SA correction. After scanning, we acquired a three-dimensional image from 1630 *x-y* images. Figures 3(a) and (b) show *x-z* projected images [3] of fluorescent beads in epoxy resin from -30 μm to 963 μm optical depth with and without SA correction, respectively. The brightness of each image was normalized using the maximum fluorescence intensity of the beads with SA correction. With SA correction, the wavefront of the excitation light was calculated and modulated every 1.55 μm of optical-depth movement. Figure 3(b) clearly shows that the fluorescence intensity of the fluorescent beads observed near the surface was the highest. As the observed depth increased, the fluorescence intensity of the beads decreased and the beads elongated in the direction of their optical axis because of SA. This result indicates that the image without SA correction (Fig. 3(b)) is equivalent to that of a conventional TPM. In Fig. 3(b), the fluorescence intensity of the beads was significantly decreased with depth increment, and fluorescence was hardly observed at optical depth greater than 200 μm. On the other hand, the fluorescence intensity of the beads was maintained until 700 μm optical depth in Fig. 3(a). To enhance the visibility of the images, we adjusted the gamma value of Figs. 3(a) and 3(b). Figures 3(c) and 3(d) show the gamma-value-adjusted *x-z* projected images ($\gamma = 1.75$)

#237841 Received 9 Apr 2015; revised 11 Jun 2015; accepted 12 Jun 2015; published 17 Jun 2015

with and without SA correction, respectively. In Fig. 3(d), the depth resolution in deep regions is low because the beads were elongated. On the other hand, in Fig. 3(c), the depth resolution is improved even in deep regions because of SA correction. Figures 3(e), 3(f), 3(g), and 3(h) show magnified *x*-*z* projected images of Figs. 3(a) and (b). The brightness of each image is normalized by the respective maximum fluorescence intensity. On application of SA correction, the observed fluorescence beads were not significantly elongated from the surface to the limit of the working distance of the objective lens.

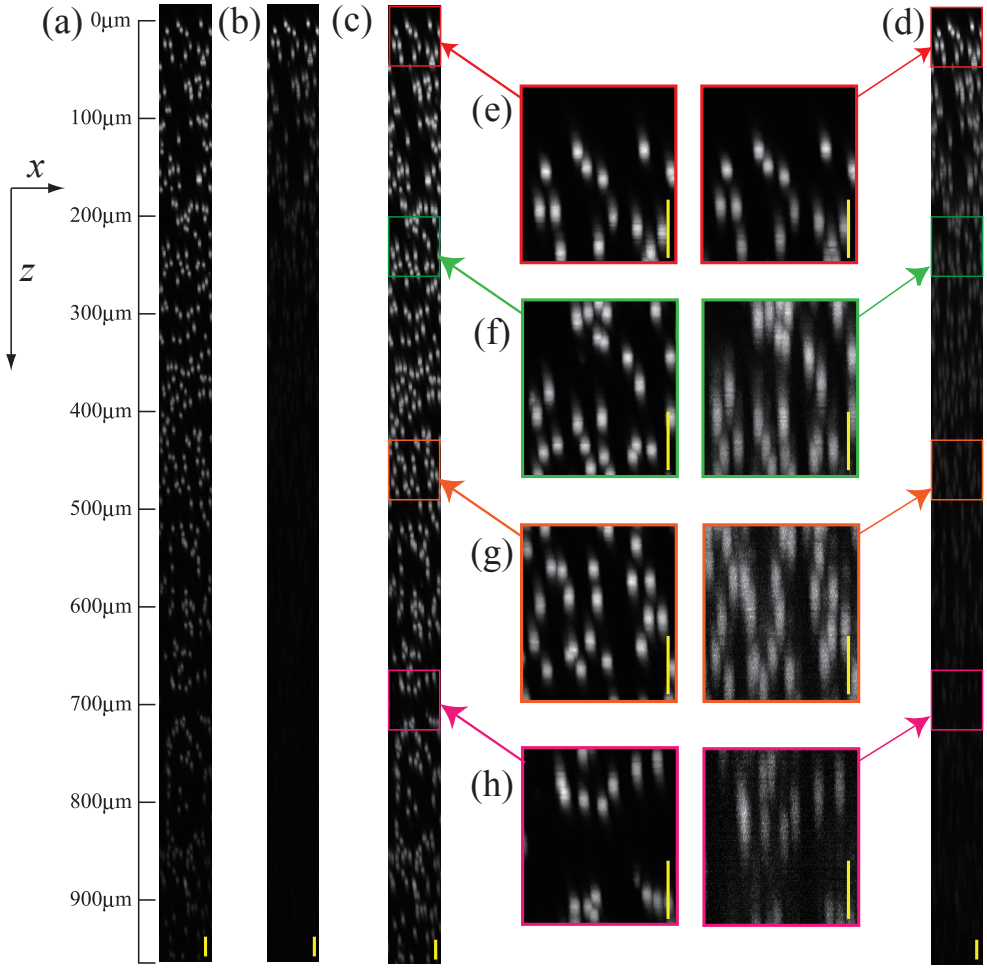

Fig. 3. Results of observation of the fluorescent polystyrene beads in epoxy resin using a dry objective lens (NA 0.75) with optical-depth increments of 621 nm. (a), (b) *x*-*z* projected image from an optical depth of -30 μm to 932 μm with and without SA correction, respectively. The 932 μm optical depth is the maximum working distance of the objective lens. (c), (d) Gamma-value-adjusted *x*-*z* projected images (γ =1.75). (e)-(f) Magnified *x*-*z* projected images from an optical depth of (e) -30 μm to 30 μm, (f) 203 μm to 263 μm, (g) 436 μm to 496 μm, and (h) 670 μm to 730 μm. Scale bar indicates 20 μm optical depth.

#237841 Received 9 Apr 2015; revised 11 Jun 2015; accepted 12 Jun 2015; published 17 Jun 2015

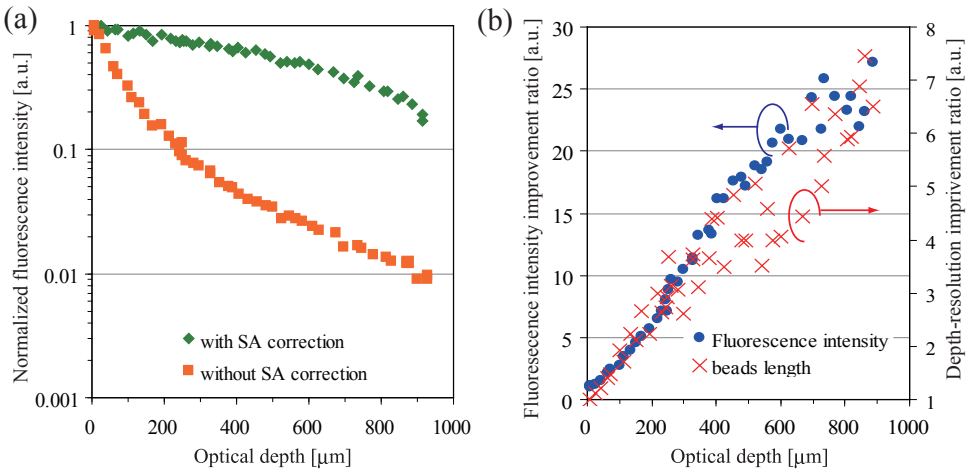

Fig. 4. (a) Normalized fluorescence intensity as a function of observed depth. (b) Fluorescence intensity improvement ratio and depth-resolution improvement ratio.

Next, we quantitatively examined the fluorescence intensity and length of the observed beads. Figure 4(a) shows the normalized fluorescence intensity of the observed beads as a function of the optical depth with and without SA correction. After the background signal was subtracted from the fluorescence intensity at each optical depth, the normalized fluorescence intensity was calculated as the fluorescence intensity at each depth divided by that near the surface of the epoxy resin. The fluorescence intensity of the beads near the surface did not vary with SA correction, because the impact of SA is negligibly small. The optical depth at which the fluorescence intensity became half of that near the surface was approximately 600 μm and 55 μm depth with and without SA correction, respectively. At 885 μm depth, the normalized fluorescence intensity improved from 0.009 to 0.232 on application of SA correction. The background signal (noise) was approximately 0.008 from the surface of the epoxy resin to the limit of the working distance of the objective lens. Figure 4(b) shows the ratio of fluorescence intensity with SA correction to that without SA correction. The fluorescence intensity with SA correction is approximately 27 times higher than that without SA correction at approximately 885 μm depth.

We defined the length of the beads as the range across which the intensity of the observed beads is greater than e^{-2} times the maximum intensity. At 7 μm depth, the lengths of the beads with and without SA correction are 9.3 μm and 8.7 μm, respectively. At 885 μm depth, the lengths of the beads with and without SA correction are 11.2 μm and 72.7 μm, respectively. Figure 4(b) also shows the improvement in depth resolution as the ratio of the length of the observed fluorescence beads with SA correction to that without SA correction. The length of the observed fluorescent beads with SA correction is approximately 6.5 times less than that without SA correction at approximately 885 μm depth.

The peak-to-valley (PV) value (stroke) of SA calculated for observation at 885 μm depth was approximately 18 μm. We confirmed with propagation simulation calculation that the fluorescence intensity with SA correction at this depth is approximately 57 times higher than that without SA correction. We consider that the difference between the experiment and the simulation comes from the residual higher order aberrations, absorption and scattering in the sample, and the characteristics of diffraction efficiency of the SLM.

#237841 Received 9 Apr 2015; revised 11 Jun 2015; accepted 12 Jun 2015; published 17 Jun 2015

4.2. *Fluorescent polystyrene beads of 3 μm diameter in a biological sample*

Fluorescent polystyrene beads of 3 μm diameter were injected into pig meat using a needle-free injector (MadaJet, Mada). Following injection of the beads, the optical transparency of the pig meat was enhanced by Scale A2 (n_2 = 1.38) [11]. Figure 5(a) gives an overall view of the pig meat after the transparency-enhancement process. Figure 5(b) shows the fluorescence image of the beads in pig meat obtained through epi-illumination. To make the interface flat, the pig meat was pressed against the cover glass. As with the observation of 3 μm-diameter fluorescent polystyrene beads in epoxy resin, we scanned the polystyrene beads using the dry objective lens with the intensity of the excitation light fixed at 6.4 mW. We observed the fluorescent beads from an optical depth of 27.6 μm to 387 μm with increments of 690 nm. Figures 5(c) and 5(d) show the *x*-*z* projected image of fluorescent beads in the pig meat with and without SA correction, respectively. Figures 5(e) and 5(f) show gamma-value-adjusted *x*-*z* projected images (γ=1.5) with and without SA correction, respectively. The fluorescence intensity of each image

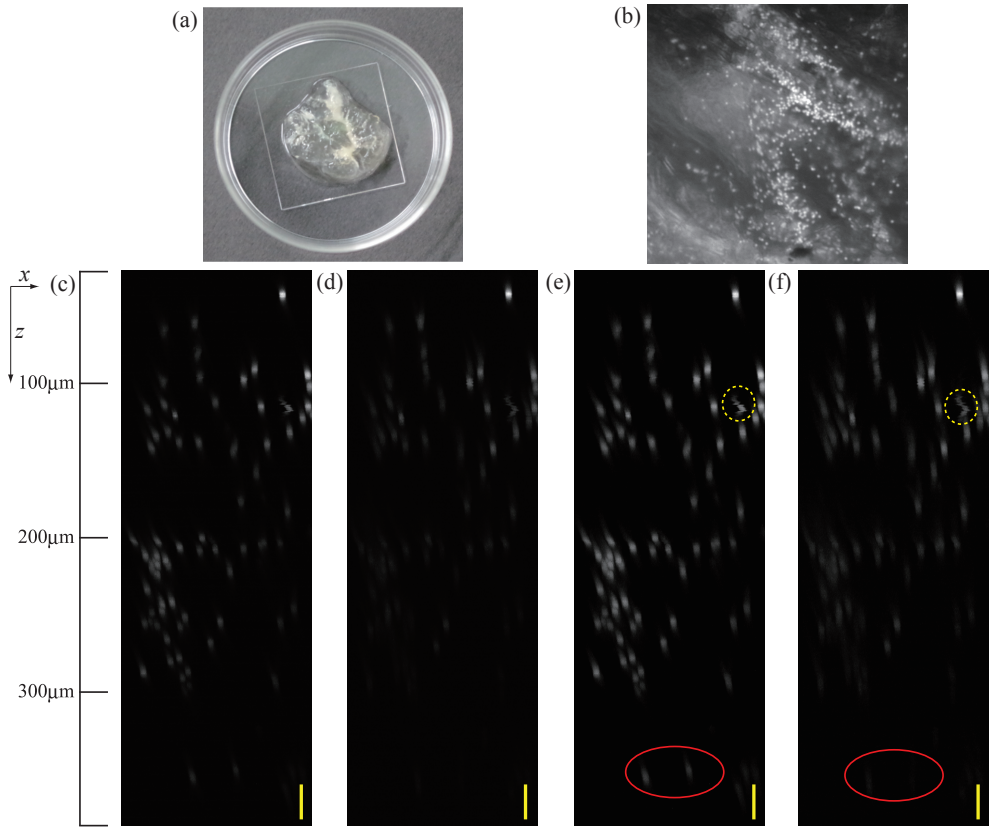

Fig. 5. Observation of fluorescent polystyrene beads in pig meat using a dry objective lens (NA 0.75) with optical-depth increments of 690 nm. (a) Overall view of the pig meat after the transparency-enhancement process. (b) *x*-*y* fluorescence image of the beads in the pig meat obtained through epi-illumination. (c), (d) *x*-*z* projected image from 27.6 μm depth to 387 μm depth with and without SA correction, respectively. (e), (f) Gamma-value-adjusted *x*-*z* projected images (γ = 1.5). Most of the fluorescence beads were fixed, but some beads moved (in the yellow dashed circle), because they were injected by a needle-free injector. Scale bar indicates 20 μm optical depth.

#237841 Received 9 Apr 2015; revised 11 Jun 2015; accepted 12 Jun 2015; published 17 Jun 2015

is normalized by the maximum fluorescence intensity of the beads with SA correction. Unlike the case with the epoxy resin, because the biological sample produced various aberrations in addition to SA, some of the beads observed in the shallow region were weaker than those in the deeper region. However, with application of SA correction, the fluorescence intensity of the observed beads became higher than that without SA correction in the deeper region. At approximately 354 μm depth (red circle in Figs. 5(e) and 5(f)), the fluorescence intensity of the beads with SA correction was approximately 5.3 times higher than that without SA correction. The length of the fluorescent beads with SA correction was approximately 2.2 times less than that without SA correction at approximately 354 μm depth.

4.3. Cerebral blood vessels of a young Sprague-Dawley rat stained with a fluorescence tracer

We also observed the cerebral blood vessels of a Sprague-Dawley (SD) rat by injecting a fluorescence tracer (Fluorescein Isothiocyanate-Dextran FD-10S, Simga Aldrich) into the circulatory system of a 7-day-old rat. The procedure was operated similar to the method used in Ref. [3]. Following injection of the fluorescence tracer, the optical transparency of the SD rat was enhanced by Scale A2 (n2 = 1.38) [11]. To make the interface flat, the sample was pressed against the cover glass. We scanned the cerebral vessels using the dry objective lens when the excitation-light intensity was fixed at 215 mW at the sample position. At each depth, scanning with SA correction was performed after scanning without SA correction. Figures 6(a) and 6(b) show the gamma-value-adjusted *y*-*z* projected images ($\gamma = 2.0$) from 0 μm depth to 550 μm depth with and without SA correction, respectively. Figures 6(e) and 6(f) show false-color *y*-*z* projected images with and without SA correction, respectively. The fluorescence intensity and resolution of blood vessels did not vary with SA correction until 100 μm depth. However, the fluorescence intensity and resolution of blood vessels improved above 100 μm depth, and the fluorescence intensity of the vessels observed with SA correction was approximately 4.0 times higher than that without SA correction at approximately 370 μm depth. Figures 6(c) and 6(d) show magnified *y*-*z* projected images of Figs. 6(a) and 6(b), respectively. The orange arrows show the length of the observed blood vessel following scanning without SA correction. The length of the observed blood vessel with SA correction is approximately 1.5 times less than that without SA correction at approximately 165 μm depth. By applying SA correction, we clearly observed approximately 10 μm-diameter blood vessels at approximately 530 μm depth (green arrows). In contrast to the fluorescence beads in epoxy resin, the improvement in the fluorescence intensity at deeper regions was not clear in the case of the blood vessels. We consider that this is because the effects of photo-bleaching of the fluorescence tracer as well as scattering and absorption were not negligible.

#237841 Received 9 Apr 2015; revised 11 Jun 2015; accepted 12 Jun 2015; published 17 Jun 2015

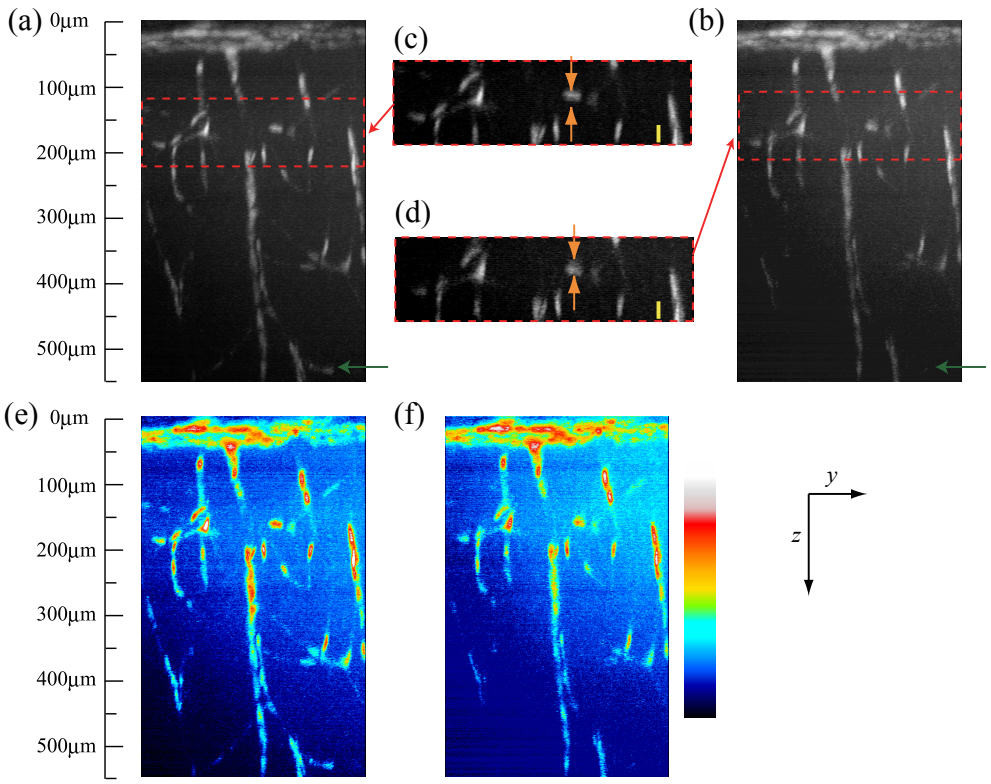

Fig. 6. Observation of the cerebral blood vessels of a young SD rat; a fluorescence tracer was injected into the circulatory system of a 7-day-old rat using a dry objective lens (NA 0.75) with optical-depth increments of 970 nm. (a), (b) *y*-*z* projected images from 0 μm depth to 550 μmm depth with and without SA correction, respectively. (c), (d) Magnified *y*-*z* projected images of (a) and (b), respectively. The orange arrows show the length of the observed blood vessel when scanned without SA correction. (e), (f) False-color *y*-*z* projected images. Scale bar indicates 20 μmm depth.

5. Discussion

SA correction using an SLM has an advantage in that the SLM suitably modulates the wavefront of the excitation light depending on the specification of the objective lens, movement of the objective lens from the interface, and the RI of the immersion medium and the average RI of the sample. Figures 7(a) and 7(b) show the *x*-*z* projected images of fluorescent beads in epoxy resin obtained using a silicone-oil immersion objective lens (30× magnification, NA 1.05, 800 μm working distance) with and without SA correction. The images were produced by scanning from an optical depth -5.5 μm to 880 μm with increments of 441 nm. Figures 7(c) and 7(d) show gamma-value-adjusted *x*-*z* projected images (γ=1.5) with and without SA correction, respectively. The RI mismatching between silicone oil (n=1.408) and epoxy resin (n $\approx$ 1.55) is less than that between air and epoxy resin. However, because the NA of the silicone-oil immersion objective lens was high, the fluorescence intensity of the observed beads in the deeper region was significantly deteriorated (Fig. 7(b)). Conversely, Fig. 7(a) indicates that the fluorescence intensity with SA correction was high in the measurement from the surface of the epoxy resin, limiting of the working distance of the objective lens.

Figure 7(e) shows the normalized fluorescence intensity as a function of the optical depth

#237841 Received 9 Apr 2015; revised 11 Jun 2015; accepted 12 Jun 2015; published 17 Jun 2015

with and without SA correction. Here, to obtain the fluorescence intensity at 0 μm, the scan was started from an optical depth of -5.6μm. An air gap was present when silicone oil was filled in the gap between the silicone-oil objective lens and the sample. The air gap vanished with increasing depth, and was refilled with silicone oil, resulting in an improved image. Because of the gap, the fluorescence intensities at 2.6 μm were lower than those at 23 μm. Figure 7(f)

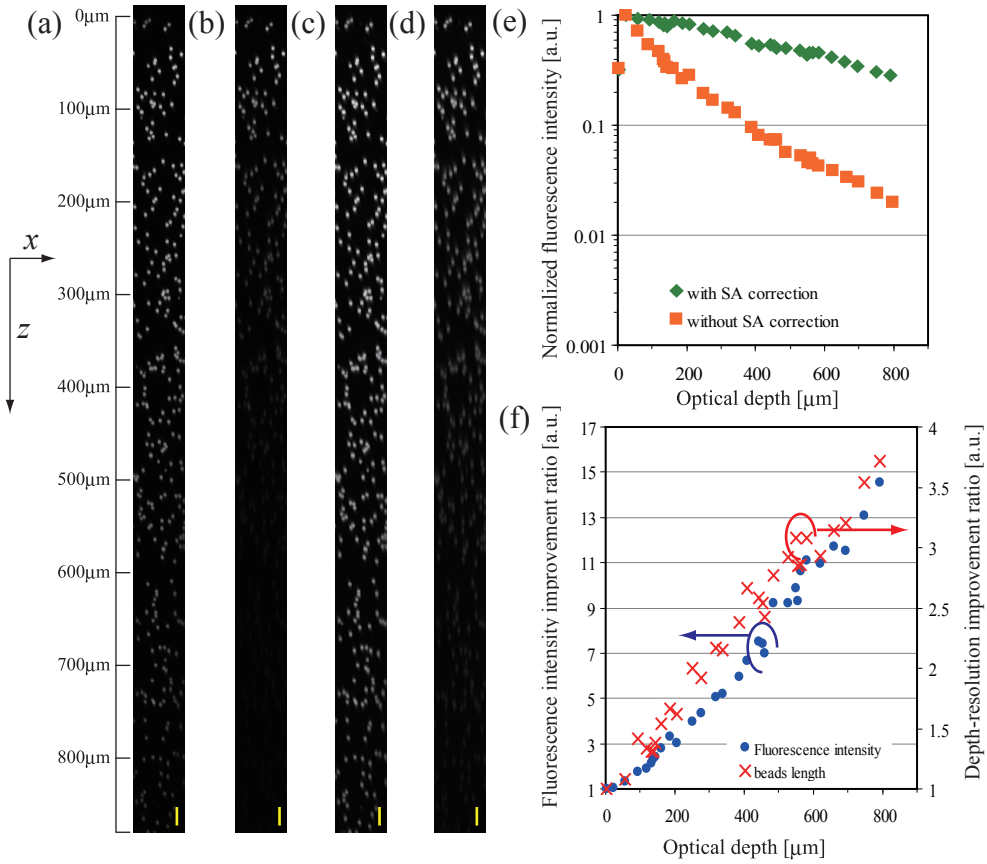

Fig. 7. Observation of fluorescent polystyrene beads in epoxy resin using a silicone-oil immersion objective lens (NA 1.05) with depth increments of 440 nm. (a),(b) *x*-*z* projected image from a depth of -5.5 μm to 880 μm with and without SA correction. (c), (d) Gamma-value-adjusted x-z projected image (γ=1.5). (e) Normalized fluorescence intensity as a function of the observed depth. (f) Fluorescence-intensity improvement ratio and depth-resolution improvement ratio. Scale bar indicates 20 μm depth.

shows the normalized fluorescence intensity as a function of the optical depth with and without SA correction. The fluorescence intensity with SA correction is approximately 14.5 times higher than that without SA correction at 792 μm depth. Figure 7(f) also shows the depth-resolution improvement ratio. At 23 μm depth, the lengths of the beads with and without SA correction are 6.2 μm and 5.7 μm, respectively. At 792 μm depth, the lengths of the beads with and without SA correction are 6.2 μm and 23.0 μm, respectively. The length of the observed beads with SA correction is 3.7 times less than that without SA correction.

The wavefront for SA correction is directly calculated, but the fluorescence-intensity improvement ratio is high in the deep region. Consequently, the intensity of the excitation light

#237841 Received 9 Apr 2015; revised 11 Jun 2015; accepted 12 Jun 2015; published 17 Jun 2015

can be reduced with SA correction because even the weak intensity of the excitation light generates sufficient fluorescence intensity for observation. By reducing the intensity of the excitation light, we expect the damage and scattering caused by fluorescence near the surface to be suppressed.

The LCOS-SLM has a large number of pixels and can modulate discontinuous phase distribution. These facts allow us to use SA correction simultaneously with other wavefront control techniques such as beam shaping [23] and generation of multifocal beam. They also allow us to use phase wrapping technique for large-stroke SA correction. In fact, we could adopt the pre-distortion pattern of 18 μm stroke in this study.

6. Conclusion

TPM with an SLM electrically corrects SA caused by RI mismatch between biological samples and the immersion medium. The modulated wavefront improves the fluorescence intensity and depth resolution of the observed fluorescence image. In this study, the wavefront was calculated using the specification of the objective lens, movement of the objective lens from the interface between the sample and the immersion medium, the RI of the immersion medium, and the average RI of the sample. The results of observation of fluorescent beads in epoxy resin using a dry objective lens with the SA correction method applied at a depth of 885 μm indicate that the fluorescence intensity was approximately 27 times higher than that without SA correction, and the length of the observed beads was 6.5 times less than that without SA correction. We also observed the beads in a biological sample (pig meat) and the cerebral blood vessels of a young rat. In future work, we plan to incorporate the SLM into an upright microscope system and use excitation light and fluorescence with longer wavelengths to reduce the scattering and absorption [2, 3, 10].

Acknowledgments

We are grateful to S. Terakawa, K. Kadomatsu, A. Hiruma, H. Toyoda, and T. Hara for their encouragement and T. Miwa, N. Fukuchi, K. Nakamura, and H. Tanaka for their invaluable assitance. This work was partially supported by SENTAN, JST.

#237841 Received 9 Apr 2015; revised 11 Jun 2015; accepted 12 Jun 2015; published 17 Jun 2015